Journal of Computational Physics 229 (2010) 6084–6103

Contents lists available at ScienceDirect

Journal of Computational Physics

journal homepage: www.elsevier.com/locate/jcp

Stochastic finite difference lattice Boltzmann method for steady incompressible viscous flows

S.C. Fu [a,*], R.M.C. So [b,c], W.W.F. Leung [d]

[a] Mechanical Engineering Department, Hong Kong Polytechnic University, Hung Hom, Hong Kong, PR China
[b] Building Services Engineering Department, Hong Kong Polytechnic University, Hung Hom, Hong Kong, PR China
[c] Mechanical Engineering Department, Purdue University, West Lafayette, IN 47907, USA
[d] Research Institute of Innovative Products and Technologies, Hong Kong Polytechnic University, Hung Hom, Hong Kong, PR China

ARTICLE INFO

Article history:
Received 16 June 2009
Received in revised form 1 March 2010
Accepted 26 April 2010
Available online 29 April 2010

Keywords:
Stochastic
Finite difference lattice Boltzmann method
Incompressible Navier–Stokes

ABSTRACT

With the advent of state-of-the-art computers and their rapid availability, the time is ripe for the development of efficient uncertainty quantification (UQ) methods to reduce the complexity of numerical models used to simulate complicated systems with incomplete knowledge and data. The spectral stochastic finite element method (SSFEM) which is one of the widely used UQ methods, regards uncertainty as generating a new dimension and the solution as dependent on this dimension. A convergent expansion along the new dimension is then sought in terms of the polynomial chaos system, and the coefficients in this representation are determined through a Galerkin approach. This approach provides an accurate representation even when only a small number of terms are used in the spectral expansion; consequently, saving in computational resource can be realized compared to the Monte Carlo (MC) scheme. Recent development of a finite difference lattice Boltzmann method (FDLBM) that provides a convenient algorithm for setting the boundary condition allows the flow of Newtonian and non-Newtonian fluids, with and without external body forces to be simulated with ease. Also, the inherent compressibility effect in the conventional lattice Boltzmann method, which might produce significant errors in some incompressible flow simulations, is eliminated. As such, the FDLBM together with an efficient UQ method can be used to treat incompressible flows with built in uncertainty, such as blood flow in stenosed arteries. The objective of this paper is to develop a stochastic numerical solver for steady incompressible viscous flows by combining the FDLBM with a SSFEM. Validation against MC solutions of channel/Couette, driven cavity, and sudden expansion flows are carried out.

1. Introduction

The Bhatnagar–Gross–Krook (BGK)-type modeled Boltzmann equation [1] has long played an important role in the development of kinetic-theory based numerical schemes. Through the use of the Chapman–Enskog or multi-scale expansion in terms of the Knudsen number, both the Euler and the Navier–Stokes (NS) equations can be derived [2]. The procedure leads to the development of numerical schemes along this direction for different types of fluid flows. Lattice Boltzmann method (LBM) is the most notable and widely used among these numerical schemes, and it has developed into an alternative and promising avenue for modeling fluid physics and simulating fluid flows [3]. The equation is hyperbolic and can be solved locally, explicitly, and efficiently on parallel computers [4,5]. Its simplicity renders the equation easy to program and to

* Corresponding author.
E-mail addresses: mm.scfu@polyu.edu.hk, fu.sau-chung@graduate.hku.hk (S.C. Fu).

0021-9991/$ - see front matter © 2010 Elsevier Inc. All rights reserved.
doi:10.1016/j.jcp.2010.04.041

incorporate the modeling of additional physical phenomena that closely mimic real physics. LBM can be considered as a particular discretization of the discrete Boltzmann equation [6,7]; therefore, the discrete Boltzmann equation can be solved by any finite difference scheme. This leads to the development of a finite difference lattice Boltzmann method (FDLBM) [7–9] that is different from the conventional LBM. Consequently, it is possible to remedy the constraint of lattice symmetry and numerical instability of the conventional LBM [7]. Recently, Fu et al. [9] have developed an FDLBM that provides a convenient algorithm for setting the boundary condition by using a splitting approach to solve the discrete Boltzmann equation. Their FDLBM is capable of simulating flows of Newtonian and non-Newtonian fluids, with or without external body forces. Also, the inherent compressibility effect of the conventional LBM, which might produce significant errors in some incompressible flow simulations, is eliminated. Through this numerical approach, a wide variety of governing equations can be similarly treated. Although the work of Fu et al. [9] was originally aimed at the simulation of micro-channel flow of power-law fluids, its application is quite broad; extension to rheological flows with built in uncertainty is a possibility.

A numerical method that can handle uncertainty is essential to providing a realistic picture for complex physical systems, because various uncertainties, such as lack of knowledge of system forcing, initial and boundary conditions, parametric uncertainties in the physical model, are unavoidable in these systems. Problems involving uncertainty are typically solved by employing Monte Carlo (MC) numerical schemes [10] which basically perform deterministic simulations with randomly input conditions, and then conduct a statistical analysis on the simulation results to extract relevant statistical properties to account for the uncertainty. The validity and extent of the calculated statistical properties depend on how large a population of simulations has been conducted. This approach is robust and is able to deal with complex situations; however, it is very CPU cost and storage demanding, so it is restricted to problems involving a small number of uncertain parameters and/or degrees of freedom only. Also, this approach does not readily provide information on the sensitivity of model outputs to specific parametric uncertainties.

Besides the MC schemes, among the available UQ methods used to simulate complicated systems with incomplete knowledge and data, the polynomial chaos (PC) based methods [11–14] are receiving growing interest because they yield accurate predictions of the uncertainty at a small fraction of the cost of a MC approach, and they provide a rich uncertainty characterization. The PC based methods for UQ have been regularly improved and applied to problems with increasing complexity since the early work of Ghanem and Spanos [14–19]; an example is their spectral stochastic finite element method (SSFEM) [14]. The essential concept in the SSFEM is to regard uncertainty as generating a new dimension and the solution as being dependent on this dimension. A convergent expansion along the new dimension is then sought in terms of the polynomial chaos system, and the coefficients in this representation are determined through a Galerkin approach. Following the idea of SSFEM, Le Maître et al. [16] developed a stochastic projection method (SPM) focusing on fluid flow problems. The method combines a Galerkin procedure for the determination of PC coefficients with a projection method for solving the incompressible Navier–Stokes (NS) equations coupled by a temperature equation. They found that only a small number of terms in the spectral expansion are required to ensure accurate representation. Also, fast convergence of the spectral representation lends credence to the potential of this approach to becoming an efficient stochastic solver. Their SPM has been generalized to account for stochastic input generated by a random process [17].

Since the FDLBM is much more efficient to solve than the finite difference solution of the NS equations, it is desirable to develop a numerical method that contains both the advantages of the FDLBM and the SSFEM or the SPM. Therefore, the objective of this paper is to develop a stochastic numerical solver for steady incompressible NS equations by combining the FDLBM with SSFEM or SPM. The numerical procedure follows that for the FDLBM outlined in [9] and the dependent variables are projected to the Homogeneous Chaos (HC) by the expansion of PC. All advantages of the FDLBM are retained. This new numerical technique is designated SFDLBM for short. Due to the simplicity of the FDLBM, the SFDLBM could offer an attractive alternative to the stochastic NS equation method proposed by Le Maître et al. [16,17]. The accuracy of the SFDLBM depends on the order of the HC used. The stochastic scheme reverts to its deterministic counterpart at zero-order of the HC.

One justification for the development of the SFDLBM is its application to simulate blood flow in micro and stenotic arteries. Blood flow has three distinct characteristics. The first is the rheological properties of blood; changes of blood rheology have been reported in several human cardiovascular diseases [20–23], but the exact mechanism of rheological changes is still not clear. The second is the pulsatile nature of the flow due to pulsating pressure, while the third is the changing boundary geometry due to plaque and cholesterol buildup inside arteries [24]. If this type of complicated non-Newtonian fluid flow were to be simulated successfully, a numerical solver that possesses the unique property of being able to simulate non-Newtonian fluids in a pulsating environment with complex boundary geometry is required. In view of this, the use of a deterministic approach to simulate blood flow might not be too appropriate. One suggestion is to adopt the MC approach [10]; however, this is limited by the size of the population that can be considered and will entail a lot more computer resource as will be shown later. Another alternative is to utilize the stochastic approach of Le Maître et al. [16,17]. This approach requires modifying the NS equations so that they can be used to treat non-Newtonian fluid flows. Due to complex geometry change as a result of plaque/cholesterol buildup, solving the blood flow problem using NS equations will either require a grid generation technique [25] or the implementation of the immersed boundary (IB) method [26], which is capable of handling complex boundary geometry. A third approach is the adoption of FDLBM, because it is simple and computationally efficient [4,5]. Even though this approach has been shown to be capable of handling non-Newtonian fluid flows having a power law viscosity in micro-channel flows [9], it still requires extension to rheological flows, where the stress strain relation is most likely nonlinear. On the other hand, the IB method [26] can be implemented into the FDLBM to give a FDLBM/IB scheme to treat flow in constricted tubes; this work is currently being attempted. If the SSFEM [14] or SPM [16] can be readily imple-

mented into FDLBM to yield a stochastic FDLBM (or SFDLBM) then a viable building block to construct a SFDLBM with IB capability is readily available. This paper attempts to construct such a SFDLBM in order to pave the way to the eventual development of a SFDLBM with IB capability (i.e. a SFDLBM/IB method). Extension to rheological fluid flows can then be carried out by further modifying the approach of [9] to treat fluid stresses with nonlinear strain rate behavior.

Another justification for the current work is the extension of the proposed SFDLBM to treat aerodynamic flows around randomly oscillating airfoils/air wings or other streamline/bluff bodies, and turbulent flows. This application also requires the implementation of the IB method into the FDLBM; such an investigation is presently being carried out. Therefore, a readily available SFDLBM could facilitate the development of this application also. Direct numerical simulation of turbulent flows is currently limited by computer capacity, thus putting an upper limit on the highest Reynolds number (Re) flow that can be simulated. The FDLBM, like the NS equations, is valid for all Re. Once a SFDLBM is available, it can be used to treat flows where the velocity and pressure fields are random processes. In other words, the formulation could be extended to simulate turbulent flows. This eventual objective needs systematic development; the present attempt is a first step towards this eventual goal. If the SFDLBM were to be used to achieve this objective, its ability to treat stochastic problems involving a random process has to be demonstrated. Therefore, it is important to show in the present study that any viable SFDLBM can handle uncertainty that is represented by a random process.

The formulation of the SFDLBM is presented in the next section. It is followed by validating the scheme against a number of numerical examples. First, the SFDLBM is validated against flow with only one random excitation; a channel/Couette flow and a driven cavity flow with viscosity as the only randomness are attempted. Next, the method is extended to flow cases with more than one source of random excitations. Simulations of a driven cavity flow and a sudden expansion flow are carried out to demonstrate this capability of the SFDLBM. Finally, the SFDLBM is used to solve flow problems involving a random process. For all cases attempted, SFDLBM results are compared with those obtained from the MC numerical scheme. Since the MC simulations are carried out under the same numerical and physical conditions, the time required for the SFDLBM and MC calculations is compared to determine the relative merit of these numerical approaches.

2. Formulation of the stochastic FDLBM (SFDLBM)

In this section, the governing equations for a 2-D steady incompressible flow are first given; it is then followed by a brief discussion of the FDLBM and the implementation of the SSFEM/SPM into the FDLBM. Finally, the numerical solution of the equations governing the SFDLBM is described.

2.1. The governing equations

As a first attempt, the focus of this paper is restricted to the solution of the two-dimensional (2-D) isothermal, incompressible NS equations, which can be written in conservation form as

$$\frac{\partial u}{\partial x}+\frac{\partial v}{\partial y}=0, \tag{1}$$

$$\frac{\partial \rho u}{\partial t}+\frac{\partial \rho u^2+p-\tau_{xx}}{\partial x}+\frac{\partial uv-\tau_{xy}}{\partial y}=0, \tag{2a}$$

$$\frac{\partial \rho v}{\partial t}+\frac{\partial \rho vu-\tau_{xy}}{\partial x}+\frac{\partial \rho v^2+p-\tau_{yy}}{\partial y}=0. \tag{2b}$$

For Newtonian fluid, the normal and shear stresses are given by

$$\tau_{xx}=2\mu\frac{\partial u}{\partial x},\quad \tau_{yy}=2\mu\frac{\partial v}{\partial y},\quad \tau_{xy}=\mu\left(\frac{\partial u}{\partial y}+\frac{\partial v}{\partial x}\right), \tag{3}$$

where μ, ρ, (u, v), p and τ_{xx}, τ_{yy}, τ_{xy}, are the viscosity coefficient, the density, the x- and y-direction velocity components, the pressure, and the viscous stress components of the flow, respectively. All variables in these equations are dimensionless, and the characteristic scales used for length, velocity, time, pressure, density, and viscosity are: L, U_∞, L/U_∞, $\rho_\infty U_\infty^2$, ρ_∞, and μ_∞, respectively. Recently, Fu et al. [9] proposed a FDLBM for steady incompressible NS equations. The scheme is originally aimed at micro-channel flows, but it is in fact applicable to a wide variety of incompressible flows. It solves the BGK-type modeled Boltzmann equation that recovers the incompressible NS equations with a convenient way to apply the boundary conditions for the governing equations, while, at the same time, retains all the advantages of the LBM.

2.2. The stochastic FDLBM (SFDLBM)

It was shown in [9] that solving the discrete particle distribution function f_α in

$$\frac{\partial f_\alpha}{\partial t}+\xi_\alpha\cdot\nabla_{\vec{x}} f_\alpha=-\frac{1}{\varepsilon\phi}(f_\alpha-f_\alpha^{eq}), \tag{4}$$

with an appropriate discrete particle equilibrium distribution function f_α^{eq} is equivalent to solving the incompressible NS equations, Eq. (1–2). In Eq. (4), the symbols ε and ϕ are a small parameter and the relaxation time, respectively, and $\varepsilon\phi = \Delta t$ is chosen. A specific D2Q9 lattice model is used and the lattice velocities ξ_α are defined as

$$\xi_0 = (0,0), \quad \alpha = 0, \tag{5a}$$

$$\xi_\alpha = c(\cos[\pi(\alpha-1)/4], \sin[\pi(\alpha-1)/4]), \quad \alpha = 1,3,5,7, \tag{5b}$$

$$\xi_\alpha = \sqrt{2}c(\cos[\pi(\alpha-1)/4], \sin[\pi(\alpha-1)/4]), \quad \alpha = 2,4,6,8, \tag{5c}$$

where c is a scaling parameter to be defined later. Details of the numerical procedure of the FDLBM scheme can be found in [9]. In this paper, the FDLBM is built into a stochastic numerical solver through application of either the SSFEM [14] or the SPM [16], and using the same procedure as that given in [9]. The SFDLBM scheme thus developed is primarily for steady flow, but as stated in [9], it can be extended to a time-accurate scheme by treating the temporal term as a pseudo-time term, which vanishes at convergence at each physical time step.

It is assumed that the source of random excitation can be written as

$$\theta_i = \theta_{i0} + \zeta_i \theta_{i1}, \tag{6}$$

where θ_i is any uncertain physical property or parameter such that its measured statistical data is a normal distribution with mean value θ_{i0} and standard deviation θ_{i1}, and ζ_i are uncorrelated Gaussian variables having zero expectation and unit variance. Theoretically, there is no restriction on the number of random excitation sources, and it is only limited by the computational resource available for a practical calculation. The source of random excitation can be an initial condition, a boundary condition, fluid properties such as viscosity coefficient, and flow properties such as driven velocity, volumetric inflow.

The expectation of a quantity g, $\langle g \rangle$, can be defined as

$$\langle g \rangle = \frac{1}{(2\pi)^{D/2}} \int_{-\infty}^{\infty} g(\zeta_i) \exp\left(-\frac{|\zeta|^2}{2}\right) \prod_i d\zeta_i. \tag{7}$$

Here, it should be pointed out that ζ is a vector with dimension D and ζ_i is its index form with index i running from 0 to $D-1$. However, it could also be a scalar as later analysis will demonstrate. By this definition of expectation, it can be easily verified that $\langle \zeta_i \rangle = 0$, $\langle \zeta_i^2 \rangle = 1$, $\langle \theta_i \rangle = \theta_{i0}$ and $\langle (\theta - \theta_{i0})^2 \rangle = \theta_{i1}^2$. Next, the dependent variables are projected to HC [11,14] by using the PC and expanding them up to M,

$$h = \sum_{i=0}^{M} h_i \Psi_i(\zeta), \tag{8}$$

where h stands for the discrete distribution function f_α, the discrete equilibrium distribution f_α^{eq}, the velocity (u, v), the pressure p and the viscous stress tensor τ_{ij}. The final representation of the flow problem can be understood by its means (expectation) as $\langle h \rangle = h_0$ and its variance as $\langle (h - h_0)^2 \rangle$. Detailed expressions for the polynomial chaoses Ψ_k can be found in [14]. The 1-D and 2-D polynomial chaoses and their variances are quoted in Tables A.1 and A.2 in Appendix A for easy reference.

Multiplying Eq. (4) with respect to Ψ_k and taking expectation using Eq. (7), the following is obtained,

$$\frac{\partial f_{\alpha k}}{\partial t} + \xi_\alpha \cdot \nabla f_{\alpha k} = -\frac{1}{\varepsilon\phi}(f_{\alpha k} - f_{\alpha k}^{eq}), \tag{9}$$

where $f_{\alpha k}^{eq}$ has also been projected to HC with every term defined as

$$f_{\alpha k}^{eq} = A_{\alpha k} + \xi_{\alpha x} Ax_{\alpha k} + \xi_{\alpha y} Ay_{\alpha k} + \xi_{\alpha x}^2 Bxx_{\alpha k} + \xi_{\alpha y}^2 Byy_{\alpha k} + \xi_{\alpha x}\xi_{\alpha y} Bxy_{\alpha k}. \tag{10}$$

The constraints for $f_{\alpha k}^{eq}$ are

$$\sum_{\alpha=0}^{8} f_{\alpha k}^{eq} = \rho_k, \text{ or } \sum_{\alpha=0}^{8} f_{\alpha 0}^{eq} = \rho, \ \sum_{\alpha=0}^{8} f_{\alpha i}^{eq} \langle \Psi_i^2 \rangle = 0, \quad i \geqslant 1, \tag{11a}$$

$$\sum_{\alpha=0}^{8} f_{\alpha k}^{eq} \xi_{\alpha x} = \rho u_k, \quad \sum_{\alpha=0}^{8} f_{\alpha k}^{eq} \xi_{\alpha y} = \rho v_k, \tag{11b,c}$$

$$\sum_{\alpha=0}^{8} f_{\alpha k}^{eq} \xi_{\alpha x}^2 = \rho \sum_{i,j} u_i u_j \frac{\langle \Psi_i \Psi_j \Psi_k \rangle}{\langle \Psi_k^2 \rangle} + p_k - \tau_{xxk}, \tag{11d}$$

$$\sum_{\alpha=0}^{8} f_{\alpha k}^{eq} \xi_{\alpha y}^2 = \rho \sum_{i,j} v_i v_j \frac{\langle \Psi_i \Psi_j \Psi_k \rangle}{\langle \Psi_k^2 \rangle} + p_k - \tau_{yyk}, \tag{11e}$$

$$\sum_{\alpha=0}^{8} f_{\alpha k}^{eq} \xi_{\alpha x}\xi_{\alpha y} = \rho \sum_{i,j} u_i v_j \frac{\langle \Psi_i \Psi_j \Psi_k \rangle}{\langle \Psi_k^2 \rangle} - \tau_{xyk}. \tag{11f}$$

It should be noted that a deterministic constant density ρ is assumed, i.e. $\rho_0 = \rho$, $\rho_k = 0$ for $k \geqslant 1$. Solving Eqs. (11a–f), the coefficients in Eq. (10) are found to be

$$A_{0k} = \rho_k - \frac{2p_k}{c^2} - \frac{\rho}{c^2}\sum_{i,j=0}^{M}(u_i u_j + v_i v_j)\frac{\langle \Psi_i \Psi_j \Psi_k\rangle}{\langle \Psi_k^2\rangle} + \frac{\tau_{xxk} + \tau_{yyk}}{c^2}, \quad A_{1k} = A_{2k} = 0, \tag{12a}$$

$$Ax_{1k} = \frac{\rho u_k}{2c^2}, Ax_{2k} = 0 \quad , Ay_{1k} = \frac{\rho v_k}{2c^2}, \; Ay_{2k} = 0, \tag{12b, c}$$

$$Bxx_{1k} = \frac{1}{2c^4}\left(p_k + \rho\sum_{i,j=0}^{M} u_i u_j \frac{\langle \Psi_i \Psi_j \Psi_k\rangle}{\langle \Psi_k^2\rangle} - \tau_{xxk}\right), \quad Bxx_{2k} = 0, \tag{12d}$$

$$Byy_{1k} = \frac{1}{2c^4}\left(p_k + \rho\sum_{i,j=0}^{M} v_i v_j \frac{\langle \Psi_i \Psi_j \Psi_k\rangle}{\langle \Psi_k^2\rangle} - \tau_{yyk}\right), \quad Byy_{2k} = 0, \tag{12e}$$

$$Bxy_{1k} = 0, \quad Bxy_{2k} = \frac{1}{4c^4}\left(\rho\sum_{i,j=0}^{M} u_i v_j \frac{\langle \Psi_i \Psi_j \Psi_k\rangle}{\langle \Psi_k^2\rangle} - \tau_{xyk}\right), \tag{12f}$$

where coefficients with the same magnitude of ξ_α are assumed equal; details of the solution procedure are given in [9].

Solving Eq. (9) and using the definitions given below,

$$u_k = \frac{1}{\rho}\sum_{\alpha=0}^{8} f_{\alpha k}\xi_{\alpha x}, \quad , v_k = \frac{1}{\rho}\sum_{\alpha=0}^{8} f_{\alpha k}\xi_{\alpha y}, \tag{13a, b}$$

$$p_k = \sum_{\alpha=0}^{8} f_{\alpha k}\frac{1}{2}\left(\xi_{\alpha x}^2 + \xi_{\alpha y}^2\right) - \frac{1}{2}\rho\left[\sum_{i,j=0}^{M}(u_i u_j + v_i v_j)\frac{\langle \Psi_i \Psi_j \Psi_k\rangle}{\langle \Psi_k^2\rangle}\right] + \frac{\tau_{xxk} + \tau_{yyk}}{2}, \tag{13c}$$

the incompressible NS equations with primitive variables (u, v, p) projected to HC are obtained.

2.3. Numerical procedure for the SFDLBM

Details of numerically solving the FDLBM are given in [9]; here only the numerical procedure used to solve the SFDLBM equations is summarized below.

(i) With the initial condition for velocity and pressure given, they are expanded in terms of the PC according to Eq. (8).
(ii) Use Eq. (10) to determine $f_{\alpha k}^{eq}$, and use it as an initial condition to solve Eq. (9).
(iii) Solve the following equation for an intermediate distribution function $f_{\alpha k}^{I}$ using any numerical scheme (this is the free streaming step),

$$\frac{\partial f_{\alpha k}}{\partial t} + \xi_\alpha \cdot \nabla f_{\alpha k} = 0. \tag{14}$$

(iv) Use $f_{\alpha k}^{I}$ and Eq. (13a–c) to find the intermediate macroscopic quantities (u_k^I, v_k^I, p_k^I) and then set the boundary condition.
(v) Use Eq. (10) to find the intermediate equilibrium distribution function $f_{\alpha k}^{I,eq}$. The intermediate equilibrium distribution function and the intermediate macroscopic quantities are in fact the evoluted values [9] (this is the collision step),

$$f_{\alpha k}|_{\vec{x},t+\Delta t} = f_{\alpha k}^{I,eq}, \tag{15a}$$

$$(u_k, v_k, p_k)|_{\vec{x},t+\Delta t} = (u_k^I, v_k^I, p_k^I). \tag{15b}$$

(vi) Repeat steps 3–5 until a steady state (conservation of mass) has been reached.

All steps in the numerical procedure are essentially the same as in the deterministic case [9] except that a series of expansion is solved and the system is enlarged by M times. When $M = 1$, or the standard deviation of the uncertain physical properties becomes zero (i.e. $\theta_{i1} = 0$), the SFDLBM reverts back to the deterministic case. After a projection to HC, Eq. (9), which is the main equation to be solved, is in a form essentially similar to Eq. (4). Also, the equations in the set are decoupled and they can be readily adapted to parallel computation. Hence, all the advantages of the FDLBM, e.g. local, explicit, and efficient for parallel computations, are retained.

3. Validation case I – only one random excitation

In order to illustrate the validity and extent of the general procedure outlined above, it would be prudent to first consider a flow with one source of random excitation. However, the relevant choice of this source needs elaboration. Blood plasma is a

non-Newtonian fluid. Its viscosity is affected by a number of factors; chief among them is the macromolecular component hematocrit (Hct). In addition, it is also influenced by the pressure, velocity, and the local shear rate of the flow [20–22]. Cholesterol and/or plaque buildup inside arteries changes the geometry of the blood vessel and in turn the pressure, velocity, and the local shear rate [23]. If the SFDLBM were to be applicable to blood flow problems, it should be able to replicate the variation of μ in real blood flow through arteries, whether micro or stenosed arteries. This means that the effect of μ variation on the flow inside blood vessels has to be reproduced correctly by the SFDLBM. Viscosity variations resulting from changes in Hct, in velocity, in pressure and in shear rate could be random in nature. In view of this, the variation of μ is a likely source of randomness to be examined first. It should be noted that Le Maître et al. [16] have also assumed μ as a source of randomness.

Blood viscosity is made up of two parts; one is due to the liquid-content and the other is due to the Hct content [20–22]. The viscosity of the liquid-content part remains relatively constant even if there are changes in shear rate, velocity and pressure. However, the viscosity of the Hct-content part is affected by these changes. This means that μ, to the lowest approximation, can be represented by Eq. (6). In a system where viscosity is the only source of randomness, $\zeta = \zeta_0$ is a scalar (i.e. $D = 1$); consequently, Eq. (6) can be re-written as

$$\mu = \mu_0 + \zeta_0 \mu_1, \tag{16}$$

(i.e., setting $\theta_0 = \mu$ in Eq. (6),) where ζ_0 is a Gaussian random variable with zero mean and unit variance. It should be noted that with the use of a Gaussian noise in the viscosity, zero or even negative values are, in principle, possible. In order to avoid this unphysical situation, the standard deviation in viscosity must be substantially smaller than the mean. In more general situations, a non-Gaussian distribution may be needed to ensure that zero or negative viscosities have negligible likelihood [16]. The appropriateness of the chosen values of the standard deviations and means in all cases of this paper is supported by the MC calculations. The expansion coefficients of the viscous stresses in Eqs. (12–13) are

$$\tau_{xxk} = 2\mu_0 \frac{\partial u_k}{\partial x} + 2\mu_1 \sum_{j=0}^{M} \frac{\partial u_j}{\partial x} \frac{\langle \zeta_0 \Psi_j \Psi_k \rangle}{\left\langle \Psi_k^2 \right\rangle}, \tag{17a}$$

$$\tau_{yyk} = 2\mu_0 \frac{\partial v_k}{\partial x} + 2\mu_1 \sum_{j=0}^{M} \frac{\partial v_j}{\partial x} \frac{\langle \zeta_0 \Psi_j \Psi_k \rangle}{\langle \Psi_k^2 \rangle}, \tag{17b}$$

$$\tau_{xyk} = \mu_0 \left(\frac{\partial u_k}{\partial y} + \frac{\partial v_k}{\partial x} \right) + \mu_1 \sum_{j=0}^{M} \left(\frac{\partial u_j}{\partial y} + \frac{\partial v_j}{\partial x} \right) \frac{\langle \zeta_0 \Psi_j \Psi_k \rangle}{\langle \Psi_k^2 \rangle}. \tag{17c}$$

Two numerical examples, namely a channel flow and a cavity driven flow, are carried out to illustrate the viability and potential of the SFDLBM.

3.1. Stochastic channel/Couette flow

In order to verify the SFDLBM scheme, a channel/Couette flow, where the two parallel plates are h apart [16], is tested first. Fig. 1 shows the schematic diagram of the flow. The lower plate is assumed stationary. The computational domain is $0 \leqslant (x,y) \leqslant 1$ (i.e. $h = 1$). For a Couette flow, there is no inflow; here, a deterministic velocity profile is specified as the inflow (at $x = 0$).

$$\begin{aligned} &u_0 = yU/h + u_{ref} y(h-y), \quad u_i = 0 \; i = 1, \ldots, M \\ &v_i = 0, \quad i = 0, \ldots, M. \end{aligned} \tag{18}$$

A no-slip boundary condition (deterministic) is specified at the channel walls (at $y = 0$ and h), i.e.

$$u_i = 0, \quad v_i = 0, \quad i = 0, \ldots, M. \tag{19}$$

For the outflow boundary (at $x = 1$),

$$\frac{\partial u_i}{\partial x} = 0, \quad \frac{\partial v_i}{\partial x} = 0, \quad i = 0, \ldots, M. \tag{20}$$

Pressures at all boundaries are found by solving Eq. (2).

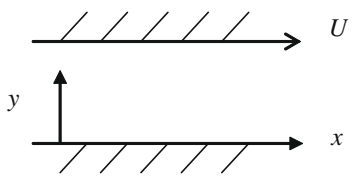

Fig. 1. Schematic diagram of the channel/Couette flow.

The above boundary settings ensure that after fully-developed flow has been achieved, $v(x,y) = 0$ everywhere, while $u = u(y)$ and $p = p(x)$; hence, a channel/Couette flow has been established. Therefore, the pressure gradient is constant and the result is given by

$$\frac{\partial p}{\partial x} = -2\mu u_{ref}. \tag{21a}$$

It can be seen that uncertainty in the viscosity affects the pressure gradient only. Setting $u_{ref} = 0.5$, $\mu_0 = 0.1$, $\mu_1 = 0.02$, Eqs. (16) and (21a) together lead to

$$\frac{\partial p_0}{\partial x}\Psi_0 + \frac{\partial p_1}{\partial x}\Psi_1 = -2\mu_{ref}(\mu_0 + \zeta\mu_1), \tag{21b}$$

and the pressure gradients for p_0 and p_1 are given by

$$\frac{\partial p_0}{\partial x} = -0.1, \quad \frac{\partial p_1}{\partial x} = -0.02. \tag{21c}$$

In the calculations, the numerical and physical parameters are specified as $\Delta x = 0.01$, $\Delta t = 0.0001$, $M = 2$, $U = 0$, 1 and 2. For this test case, the free streaming step, i.e. Eq. (14), is solved using the same LBM discretization scheme as detailed in [3,6,9]. In finite difference form, it can be written as

$$f_{\alpha k}(\vec{x} + \xi_\alpha \Delta t, t + \Delta t) = f^{eq}_{\alpha k}(\vec{x}, t). \tag{22}$$

Hence, $c = \Delta x/\Delta t = 100$. Fig. 2 shows the pressure profiles along the centerline (at $y = h/2$) of the channel in the x-direction. Only the case $U = 1$ is shown because the results of $U = 0$ and 2 are exactly the same. They are in excellent agreement with the analytical results given in Eq. (21c). This shows that the pressure gradients are calculated correctly by the SFDLBM.

3.2. Driven cavity flow with Gaussian viscosity randomness

A laminar incompressible flow in a square cavity whose top wall moves with a uniform velocity in its own plane is a typical example of a steady separated flow (Fig. 3). In spite of the singularities at two of its upper corner, driven cavity flow has served repeatedly as a model problem for testing and evaluating numerical techniques [27]. The validity and extent of the FDLBM in resolving such a problem has been demonstrated in [9]. It would be interesting to examine the effect of an uncer-

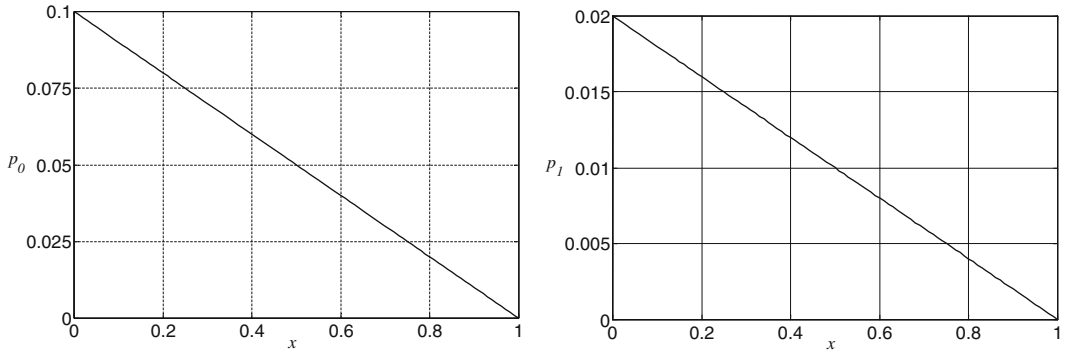

Fig. 2. Pressure profile of the stochastic channel/Couette flow problem with an uncertain viscosity along the centerline (at $y = h/2$).

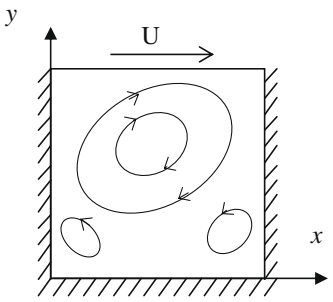

Fig. 3. Schematic diagram of the driven cavity flow.

tain viscosity on the velocity field. In order to verify the SFDLBM, the result thus obtained is compared with those deduced from the MC scheme. In the MC calculation, a large number (1000) of viscosity coefficients are generated randomly (in Gaussian). Then, the same number of cases of driven cavity flows is calculated deterministically. For a more fitting comparison, the FDLBM given in [9] is used to carry out every deterministic simulation. Also, the numerical and physical parameters of the MC simulations are set identical to those used in SFDLBM simulations.

The computational domain is defined by $0 \leqslant (x, y) \leqslant 1$. At the upper plate, the boundary condition is specified as

$$\begin{aligned} &u_0 = U, \quad u_i = 0, \quad i = 1, \ldots, M, \\ &v_i = 0, \quad i = 0, \ldots, M \end{aligned} \tag{23}$$

while a no-slip condition as stipulated in Eq. (19) is invoked for the other three walls. Again, the pressures at all boundaries are calculated according to Eq. (2). The numerical and physical parameters specified are: $\Delta x = 0.02$, $\Delta t = 0.0001$, $\mu_0 = 0.01$, $\mu_1 = 0.0025$, $U = 1$. In this case, the free streaming step, Eq. (14), is solved using the Lax–Wendroff scheme [28]. The scaling parameter in Eqs. (5a–c) is chosen according to,

$$c = K_c \sqrt{\max_{(x,y,k)} \left\{ \sum_{i,j} (u_i u_j + v_i v_j) \frac{\langle \Psi_i \Psi_j \Psi_k \rangle}{\langle \Psi_k^2 \rangle} + \frac{2p_k - \tau_{xxk} - \tau_{yyk}}{\rho} \right\}}, \tag{24}$$

where K_c is a numerical parameter which needs to be determined case by case. For most cases and in this particular example, stable and correct result is obtained by choosing $K_c = 1$. This choice of c is not unique and can be deduced from Eq. (13c), or

$$\frac{1}{2}\rho \left[\sum_{i,j} (u_i u_j + v_i v_j) \frac{\langle \Psi_i \Psi_j \Psi_k \rangle}{\langle \Psi_k^2 \rangle} \right] + p_k - \frac{\tau_{xxk} + \tau_{yyk}}{2} = \frac{\sum_{\alpha=0}^{8} f_{\alpha k} |\xi_\alpha|^2}{2} \leqslant \rho \frac{\max_\alpha |\xi_\alpha|^2}{2}. \tag{25}$$

The inequality can be ensured by choosing a large enough K_c. Numerical experiment shows that the scheme will become unstable if the choice of K_c is too small; however, it affects the convergence and accuracy if K_c is too large.

The u and v velocity plots along the center of the axes are shown in Figs. 4 and 5, respectively. Symbol 'o' is the deterministic result from Ghia et al. [27]. The solid line is the result of the deterministic solution by FDLBM, while symbols '+', '•', '*', '×' are the SFDLBM results with the order of the HC given by $M_p = 1, 2, 3, 4$, respectively. In fact, when $M = M_p = 1$ or $\mu_1 = 0$, the SFDLBM reverts to its deterministic counterpart. It should be noted that the order of the HC, M_p, is not the same as the number of terms M of the PC. For example, in 2-D PC (Table A.2 in Appendix A), when the index j is started from zero, for $M_p = 4$, M is 14. But in the 1-D case ($D = 1$), they are the same. Also, it should be noted that the solution after projected onto the HC is dependent on ζ_0, i.e., $p = p(x, y, \zeta_0)$, $u = u(x, y, \zeta_0)$, and $v = v(x,y, \zeta_0)$. The stochastic results plotted in Figs. 4 and 5 represent the values of the velocity component, defined by putting $\zeta_0 = 0$, which are not necessarily the same as the mean values (by taking expectation of Eq. (7)). As expected, the stochastic results obtained by setting $\zeta_0 = 0$ converge to the deterministic values (at mean viscosity) with increasing M_p. The figures show that all results are in agreement with those given by Ghia et al. [27] and those obtained deterministically, and this provides a verification of the SFDLBM code.

For quantitative comparison, Table 1 shows the maximum error norm between the deterministic results and the stochastic results with $\zeta_0 = 0$ (the first column), the maximum norm between the deterministic results and the mean (expectation) values deduced from SFDLBM (the second column) and the maximum variance (the third column). Since the Lax–Wendroff scheme is second order accurate, the numerical error of the method is estimated to be of $O(\Delta t, \Delta x^2 \approx 4e{-}4)$. The maximum error norms between the deterministic results and the stochastic results with $\zeta_0 = 0$ (the first column in Table 1) shows a general trend of approaching to the same order as the estimated numerical error as M_p increases and better values are

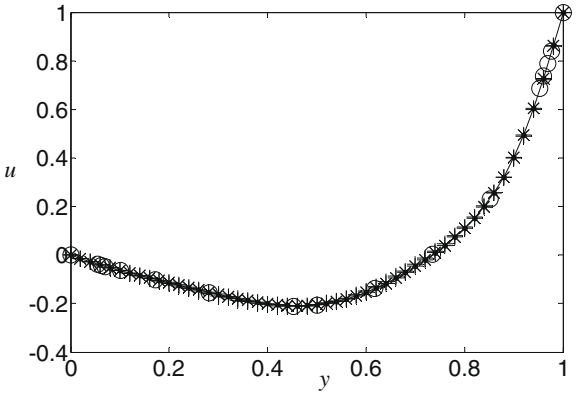

Fig. 4. Horizontal velocity, u, of driven cavity flow along y at $x = 0.5$: '—', deterministic result; '+', '•', '*', '×' are SFDLBM results by putting $\zeta_0 = 0$ with $M_p = 1$, 2, 3, 4, respectively; 'o', Ghia et al. [27] result.

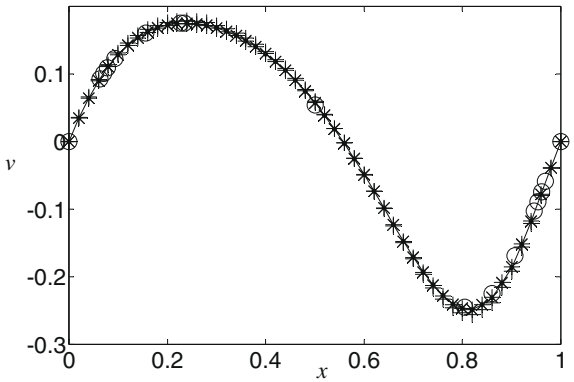

Fig. 5. Vertical velocity, v, of driven cavity flow along x at $y = 0.5$: '—', deterministic result; '+', '•', '*', '×' are SFDLBM results by putting $\zeta_0 = 0$ with $M_p = 1, 2, 3, 4$, respectively; 'o', Ghia et al. [27] result.

Table 1
The maximum norm between the deterministic results and the stochastic results. The subscript 's' is used to denote the stochastic results, and the subscript 'd' the deterministic results.

	$\max_y\lvert u_s(\zeta_0 = 0) - u_d\rvert_{x=0.5}$	$\max_y\lvert\langle u_s\rangle - u_d\rvert_{x=0.5}$	$\max_y\lvert var(u_s)\rvert_{x=0.5}$
$M_p = 1$	7.5102e−3	7.5102e−3	8.5874e−4
$M_p = 2$	2.0833e−4	7.5680e−3	1.0963e−3
$M_p = 3$	1.3844e−3	7.3939e−3	1.0549e−3
$M_p = 4$	4.4431e−4	7.3666e−3	1.0532e−3
$M_p = 5$	7.6337e−4	7.3785e−3	1.0613e−3
$M_p = 6$	3.7468e−4	6.8305e−3	9.8740e−4
	$\max_x\lvert v_s(\zeta_0 = 0) - v_d\rvert_{y=0.5}$	$\max_x\lvert\langle v_s\rangle - v_d\rvert_{y=0.5}$	$\max_x\lvert var(v_s)\rvert_{y=0.5}$
$M_p = 1$	7.4152e−3	7.4152e−3	6.3321e−4
$M_p = 2$	1.3751e−4	7.9598e−3	9.4365e−4
$M_p = 3$	1.0689e−3	7.8569e−3	9.6521e−4
$M_p = 4$	3.3690e−4	7.7230e−3	9.3652e−4
$M_p = 5$	9.4099e−4	7.6890e−3	9.2024e−4
$M_p = 6$	4.8674e−4	6.2518e−3	8.2190e−4

obtained when the HC is of even order. Also, it is observed that, increasing the order of HC only has a weak effect on the expected velocity field (the second column of Table 1). In this problem, the source of randomness is the viscosity which has a variance of $\mu_1^2 = 6.25e-6$, the calculations (the third column of Table 1) show that the resulting variance in the velocity is much larger than that of the source.

Table 2
Error norms of the driven cavity flow with viscosity as the only randomness.

	Max-norm	2-norm	1-norm
$u_s - u_{MC}$			
Deterministic	0.8647773	0.0609374	0.0298494
$M_p = 1$	0.1594504	0.0053829	0.0023014
$M_p = 2$	0.1336953	0.0024673	9.2606e−4
$M_p = 3$	0.0908352	0.0013015	4.4028e−4
$M_p = 4$	0.0390914	7.3827e−4	2.6773e−4
$v_s - v_{MC}$			
Deterministic	0.5218596	0.0424875	0.0233721
$M_p = 1$	0.1536490	0.0040369	0.0015446
$M_p = 2$	0.1137691	0.0019872	7.3293e−4
$M_p = 3$	0.0643528	9.9191e−4	3.5903e−4
$M_p = 4$	0.0261239	5.5758e−4	2.0870e−4
$p_s - p_{MC}$			
Deterministic	2.3019389	0.0401191	0.0162286
$M_p = 1$	0.0604677	0.0016002	7.9883e−4
$M_p = 2$	0.0469459	8.1678e−4	4.5270e−4
$M_p = 3$	0.0251763	5.4927e−4	3.6818e−4
$M_p = 4$	0.0136618	4.9142e−4	3.5326e−4

The results calculated by the SFDLBM are also compared with those derived from the MC scheme. An error analysis is reported in Table 2. In this paper, all error analyses are focused on the spectral stochastic method itself, i.e. the order of the HC, and not on the grid size. This is because all examples chosen in the current study have been investigated in [9]; hence, the grid chosen for the FDLBM simulation is considered appropriate for these examples. Maximum norm (max-norm) and q-norm are calculated by differencing each set of MC results, $u_{MC,j}$, with the stochastic results derived from the SFDLBM simulations, $u_{s,j}$,

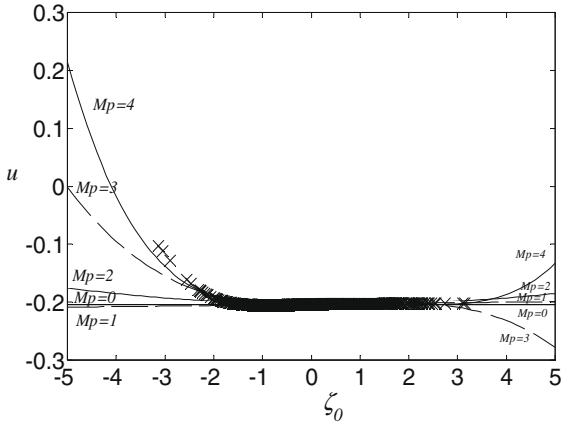

Fig. 6. Horizontal velocity, u, of driven cavity flow against ζ_0 for different M_p: '—', SFDLBM results; '×', MC result.

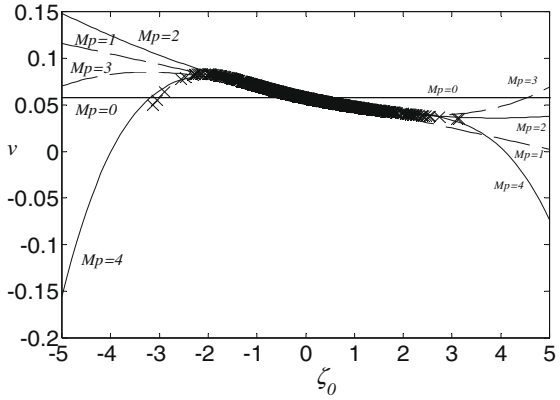

Fig. 7. Vertical velocity, v, of driven cavity flow against ζ_0 for different M_p: '—', SFDLBM results; '×', MC result.

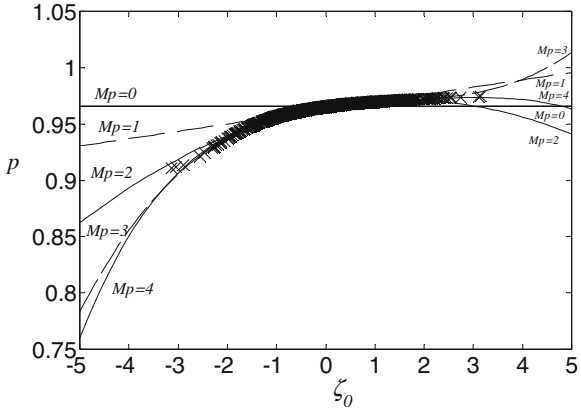

Fig. 8. Pressure, p, of driven cavity flow against ζ_0 for different M_p: '—', SFDLBM results; '×', MC result.

$$\max\text{-norm} = \max_{x,y,j} |u_{s,j} - u_{MC,j}|, \tag{26a}$$

$$q\text{-norm} = \left(\frac{1}{N\Omega} \sum_{x,y,j} |u_{s,j} - u_{MC,j}|^q \right)^{1/q}, \tag{26b}$$

where N is the number of samples specified in the MC scheme, and Ω is the area of the computational domain. In the present calculation, $N = 1000$ and $\Omega = 1$. For each MC sample, indexed by j, there is a corresponding value for ζ_0. The stochastic solution $u_{s,j}$ is obtained by putting the corresponding ζ_0 into the SFDLBM solution, $u(x, y, \zeta_0)$. In Figs. 6–8, u, v, and p are plotted against ζ_0 at the center of the cavity ($x = 0.5, y = 0.5$). The symbol '$\times$' is the MC result calculated using 1000 samples. It is seen that the higher the order of HC employed, the better the agreement is when compared with the MC results.

4. Validation case II – more than one random excitation

In this section, cases with more than one independent random excitation are considered. The number of random excitations is represented by the dimension of the Gaussian random variable ζ, which is denoted as D in Eq. (7). The case of $D = 2$ (two sources) is used as an illustrative example in this section. Calculation of higher dimension, i.e. more than two random excitations, follows the same procedure. For illustration purposes, two examples, a driven cavity flow and a sudden expansion flow, are presented below.

Fluid viscosity is still considered as one of the random excitations. The choice of a second random excitation needs some consideration. In a stenosed artery, plaque and cholesterol buildup will lead to changes in the velocity of blood flow, which in turn could contribute to a viscosity change. Therefore, a reasonable second choice of random excitations is the flow velocity. This implies that, in the cavity flow problem, both the viscosity and the upper plate velocity are considered to have a random excitation component, while in the sudden expansion flow problem the viscosity and the mean volume flow rate are assumed to have a random excitation component.

4.1. Driven cavity flow with two random excitations

For this problem, in addition to μ (i.e. Eq. (16)), it is also assumed that the velocity of the upper plate of the cavity is uncertain and can be written as

$$U = U_0 + \zeta_1 U_1, \tag{27}$$

(i.e., setting $\theta_0 = \mu$ and $\theta_1 = U$ in Eq. (6)) where ζ_1 is a Gaussian random variable similar but independent of ζ_0, sharing the same definition of expectation as given in Eq. (7). For the present example, $D = 2$ and it can be verified that $\langle \zeta_1 \rangle = 0$, $\langle \zeta_1^2 \rangle = 1$, $\langle U \rangle = U_0$ and $\langle (U - U_0)^2 \rangle = U_1^2$. Exactly the same formulation as described in the previous section is employed. The pressure and velocity, which are projected to the HC, can be calculated by using the same procedure as detailed in the previous section except that $\boldsymbol{\zeta}$ is now a vector, $\boldsymbol{\zeta} = (\zeta_0, \zeta_1)$ with components ζ_0 and ζ_1, instead of a scalar. The solution therefore depends on both ζ_0 and ζ_1, i.e. $p = p(x, y, \zeta_0, \zeta_1)$, $u = u(x, y, \zeta_0, \zeta_1)$, and $v = v(x, y, \zeta_0, \zeta_1)$. The results calculated by the SFDLBM are compared with those obtained from the MC simulation scheme. The same numerical and physical parameters as specified in the previous driven cavity flow case are used in the current simulations. Additional parameters that need to be specified are: $U_0 = 1$ and $U_1 = 0.25$. The error norms between the SFDLBM and the MC results are given in Table 3. It is seen that the error norm decreases with increasing order of the HC.

4.2. Sudden expansion flow with two random excitations

A channel with a symmetric sudden expansion gives rise to an internal separated flow. The flow geometry shown in Fig. 9 [9,29] has a parabolic profile prescribed at the entrance ($x = 0$)

$$u|_{x=0} = \frac{3q}{2h} \left[1 - \left(\frac{y}{h} \right)^2 \right], \quad 0 \leqslant y \leqslant h = 0, \ h \leqslant y \leqslant 1, \tag{28}$$

where h is the half-width of the channel upstream of the expansion. In addition to the viscosity coefficient as given in Eq. (16), the mean volume flow rate q is also considered to be an uncertainty parameter; it is defined as

$$q = q_0 + \zeta_1 q_1, \tag{29}$$

(i.e., setting $\theta_0 = \mu$ and $\theta_1 = q$ in Eq. (6)). A computational domain bounded by $0 \leqslant x \leqslant 20$, $0 \leqslant y \leqslant 1$ (i.e. $h = 0.5$) is used. The numerical and physical parameters are given by $\Delta x = 0.05$, $\Delta t = 0.0001$, $K_c = 2.5$, $q_0 = 1$, $q_1 = 0.2$, $\mu_0 = 1/(46.6) \approx 0.02146$, $\mu_1 = 0.005$. This specification gives rise to a mean Reynolds number of Re = 46.6. The same settings as in Eq. (20) are used for the outflow boundary condition. The error norms between the SFDLBM and the MC results are shown in Table 4. The results are not as good as the driven cavity flow case presented above; however, as expected, the error norm decreases as the HC order increases.

Table 3
Error norms of the driven cavity flow with two random excitations.

	Max-norm	2-norm	1-norm
$u_s - u_{MC}$			
Deterministic	0.2151781	0.0135681	0.0068239
$M_p = 1$	0.1909254	0.0086299	0.0042735
$M_p = 2$	0.1559440	0.0035074	0.0014738
$M_p = 3$	0.1129188	0.0019038	7.1737e−4
$M_p = 4$	0.0871112	0.0012729	4.7242e−4
$v_s - v_{MC}$			
Deterministic	0.2219703	0.0103100	0.0049905
$M_p = 1$	0.1917158	0.0063802	0.0028770
$M_p = 2$	0.1334582	0.0028935	0.0012443
$M_p = 3$	0.1045993	0.0015324	5.5668e−4
$M_p = 4$	0.0750158	9.5193e−4	3.8284e−4
$p_s - p_{MC}$			
Deterministic	1.0164630	0.0185207	0.0062602
$M_p = 1$	0.6209397	0.0074367	0.0032909
$M_p = 2$	0.0688347	0.0015633	7.8578e−4
$M_p = 3$	0.0819707	9.2195e−4	4.5828e−4
$M_p = 4$	0.0383901	6.1968e−4	3.6777e−4

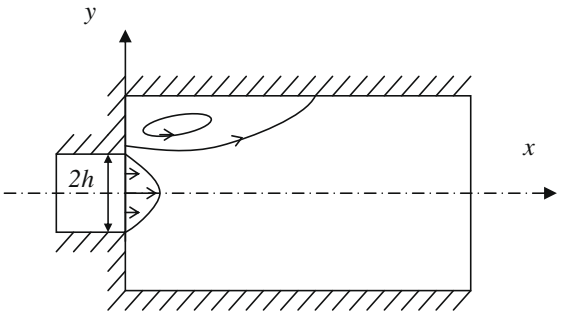

Fig. 9. Schematic diagram of the flow in a channel with a symmetric sudden expansion.

Table 4
Error norms of the sudden expansion flow with two random excitations.

	Max-norm	2-norm	1-norm
$u_s - u_{MC}$			
Deterministic	2.0086477	0.2612888	0.1730731
$M_p = 1$	1.0292877	0.0314825	0.0134520
$M_p = 2$	0.7567994	0.0142168	0.0047911
$M_p = 3$	0.4963875	0.0065793	0.0021707
$M_p = 4$	0.2091024	0.0025238	0.0011193
$v_s - v_{MC}$			
Deterministic	0.0983164	0.0054402	0.0027784
$M_p = 1$	0.0569045	0.0016440	7.4201e−4
$M_p = 2$	0.0283838	6.5860e−4	2.7004e−4
$M_p = 3$	0.0165518	3.5667e−4	1.4462e−4
$M_p = 4$	0.0084211	2.3328e−4	1.0251e−4
$p_s - p_{MC}$			
Deterministic	2.2894731	0.3044806	0.1946382
$M_p = 1$	1.0149645	0.0943119	0.0529843
$M_p = 2$	0.9868502	0.0224071	0.0089726
$M_p = 3$	0.8154958	0.0163760	0.0036862
$M_p = 4$	0.4866599	0.0109501	0.0023807

5. Validation case III – one random process

In previous sections, the viscosity coefficient, though uncertain, is treated as spatially uniform. However, this might not be the case in the flow through stenosed arteries. As indicated in [25], the mean velocity varies rapidly across and along a

constricted tube in the section where the constriction occurs. This rapid variation created by the geometry of the constriction can be simulated and tracked through the addition of a body force term in the governing momentum equation [26]. The immersed boundary method can also be incorporated into the SFDLBM through an additional distribution function in the modeled lattice Boltzmann equation; this task will be carried out later. Since blood viscosity μ is influenced by changing velocity, pressure, and shear rate [20–22], it could be argued that μ might vary substantially in the region where these changes occur. Therefore, in the constricted section, μ will not only be affected by the changing velocity, pressure, and shear rate, it might also loss its spatially uniform property.

In order to account for this geometry effect on μ, it can be treated as a random process with spatial variation given by

$$\mu(\vec{x}) = \mu_0(\vec{x}) + \mu'(\vec{x}). \tag{30}$$

The formulation developed before is in fact also appropriate for the treatment of random process. In extending the SFDLBM scheme to treat problems involving a random process, the approach of [17] is followed. The first term on the right hand side of Eq. (30) is the expectation, i.e. $\langle\mu\rangle = \mu_0$, and the second term is the random component given by an autocorrelation function K, such that

$$K(\vec{x}_1, \vec{x}_2) = \langle \mu'(\vec{x}_1)\mu'(\vec{x}_2)\rangle = \sigma^2 \exp\left(-\frac{|\vec{x}_1 - \vec{x}_2|}{L_c}\right). \tag{31}$$

It is assumed that $K(\vec{x}_1, \vec{x}_2)$ is a Gaussian process characterized by its variance σ and its normalized correlation length L_c. This means that for any two points $\vec{x}_1$ and $\vec{x}_2$, the viscosity coefficients measured are found to have a Gaussian relation as given in

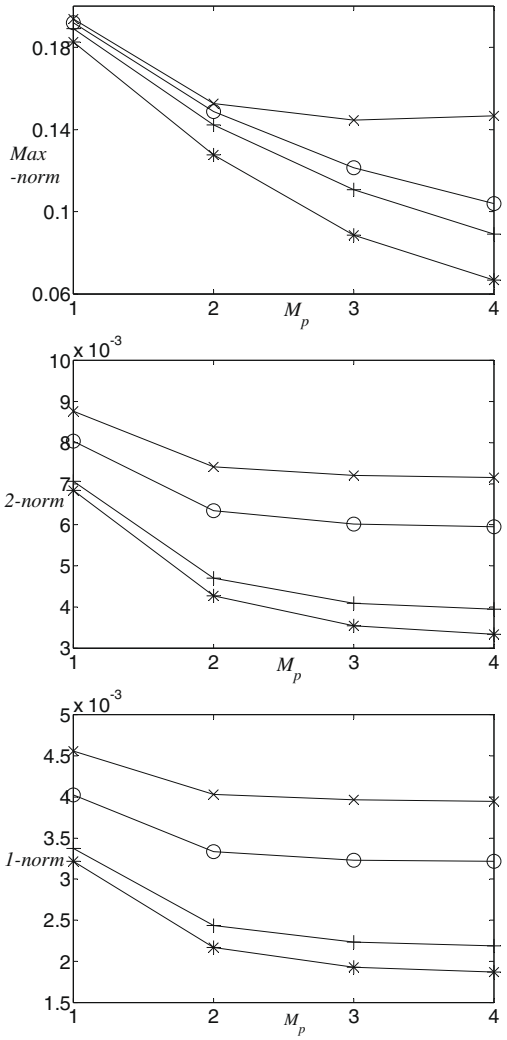

Fig. 10. Error norms of the horizontal velocity u of driven cavity flow with viscosity in random process: '×', 'o', '+', '*' are SFDLBM results with N_{KL} = 1, 2, 3, 4, respectively.

Eq. (31). The uncertainty is dependent on the independent variable, $\vec{x}$ (the space), and this is the main difference between the formulation given in this section and that presented in previous sections. The autocorrelation function can be expanded in terms of its eigenvalues λ_i and eigenfunctions f_i' [14], such that

$$K(\vec{x}_1, \vec{x}_2) = \sum_{i=0}^{\infty} \lambda_i f_i'(\vec{x}_1) f_i'(\vec{x}_2), \tag{32}$$

and μ' is expressed accordingly in the usual Karhunen–Loève (KL) expansion [14]

$$\mu'(\vec{x}) = \sum_{i=0}^{\infty} \sqrt{\lambda_i} f_i'(\vec{x}) \zeta_i, \tag{33}$$

where ζ_i are uncorrelated Gaussian variables having zero expectation and unit variance. The eigenvalues λ_i and eigenfunctions f_i' of $K(\vec{x}_1, \vec{x}_2)$ are the solutions of the corresponding integral operator [14]

$$\int_0^1 K(\vec{x}_1, \vec{x}_2) f'(\vec{x}_2) d\vec{x}_2 = \lambda f'(\vec{x}_1). \tag{34}$$

This Fredholm equation can be solved numerically; however, for the kernel given in Eq. (31) and for the 1-D spatial case, an analytical solution is available in [14]. This is given by

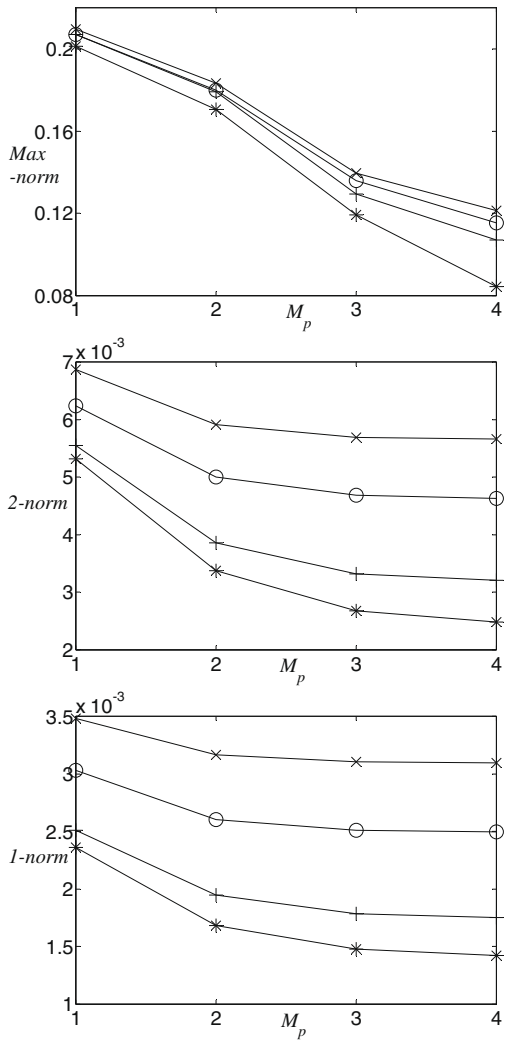

Fig. 11. Error norms of the vertical velocity v of driven cavity flow with viscosity in random process: '×', 'o', '+', '*' are SFDLBM results with N_{KL} = 1, 2, 3, 4, respectively.

$$f_n'(y) = \begin{cases} \frac{\cos[\omega_n(y-1/2)]}{\sqrt{\frac{1}{2}+\frac{\sin(\omega_n)}{2\omega_n}}} & \text{if } n \text{ is even,} \\ \frac{\sin[\omega_n(y-1/2)]}{\sqrt{\frac{1}{2}-\frac{\sin(\omega_n)}{2\omega_n}}} & \text{if } n \text{ is odd,} \end{cases} \quad \text{and,} \tag{35a}$$

$$\lambda_n = \sigma^2 \frac{2L_c}{1+(\omega_n L_c)^2}, \tag{35b}$$

where ω_n are the positive roots of the characteristic equation

$$[1 - L_c\omega\tan(\omega/2)][L_c\omega + \tan(\omega/2)] = 0. \tag{36}$$

Since the first positive root of Eq. (36) is $\omega_0 = 0$, and correspondingly $f_0' = 0$, Eq. (30) can be expressed as

$$\mu(y) = \mu_0(y) + \sum_{i=1}^{N_{KL}} \sqrt{\lambda_i} f_i'(y)\zeta_i, \tag{37}$$

where for numerical purpose, the series is truncated up to N_{KL} only. As a result, matching the dimension of ζ to the order of the KL expansion gives $D = N_{KL}$. Eq. (37) is in fact a re-write of Eq. (6) with $\theta_{00} = \theta_{01} = 0$, $\theta_{10} = \mu_0$, $\theta_{i0} = 0$, $i > 1$, and θ_{i1}, $i \geqslant 1$ being the coefficients of the KL series. The same formulation of the scheme as in the previous section can be employed.

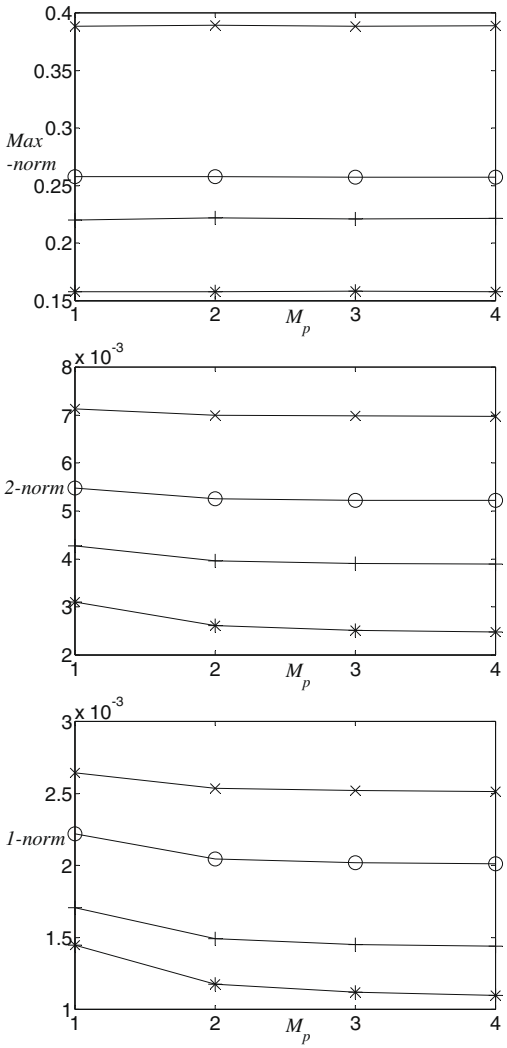

Fig. 12. Error norms of the pressure p of driven cavity flow with viscosity in random process: '×', 'o', '+', '*' are SFDLBM results with $N_{KL} = 1, 2, 3, 4$, respectively.

5.1. Driven cavity flow with viscosity as a random process

In order to verify the effectiveness of the application of the KL expansion in the SFDLBM, it is assumed that fluid viscosity μ of a driven cavity flow is a random process represented by Eq. (37) with the independent variable y replaced by r, where $r = \sqrt{(x-0.5)^2 + (y-0.5)^2}$. This implies that the uncertainty is radially symmetric about the center of the cavity. Thus, the expression given in Eq. (37) with y replaced by r represents a simple model of a random process for μ. Such a model is chosen because it permits a MC simulation to be carried out within the limited computer resource of the Department. Furthermore, as a first attempt to verify the validity and extent of the SFDLBM with μ being a random process, Eq. (37) with y replaced by r affords simplicity to allow the stated objectives of the study to be accomplished. The numerical and physical parameters specified are $\Delta x = 0.02$, $\Delta t = 0.0001$, $K_c = 1$,$\mu_0 = 0.01$, $\sigma = 0.0025$, $L_c = 1$,$U = 1$. Figs. 10–12 show the error norms of the velocity and the pressure between the SFDLBM and the MC results, where 1000 samples are used in the MC simulation scheme. Significant improvement is shown by increasing N_{KL}. The error is smaller for larger M_p, but it seems to converge and almost reach the correct result at $M_p = 4$. Therefore, N_{KL} plays a more critical role for the accuracy when M_p is sufficiently high.

Besides the uncertain μ, the speed of the upper plate of the cavity can also be considered to be uncertain. Since the index i in Eq. (37) starts from 1, by defining the speed of the upper plate as

$$U = U_0 + \zeta_0 U_1, \tag{38}$$

(i.e., setting $\theta_{00} = U_0$, $\theta_{01} = U_1$, and again $\theta_{10} = \mu_0$, $\theta_{i0} = 0$, $i > 1$, and θ_{i1}, $i \geqslant 1$ are the coefficients of the KL series in Eq. (6)) where ζ_0 is a Gaussian variable having zero expectation and unit variance and uncorrelated to other ζ_i for $i \geqslant 1$, a stochastic

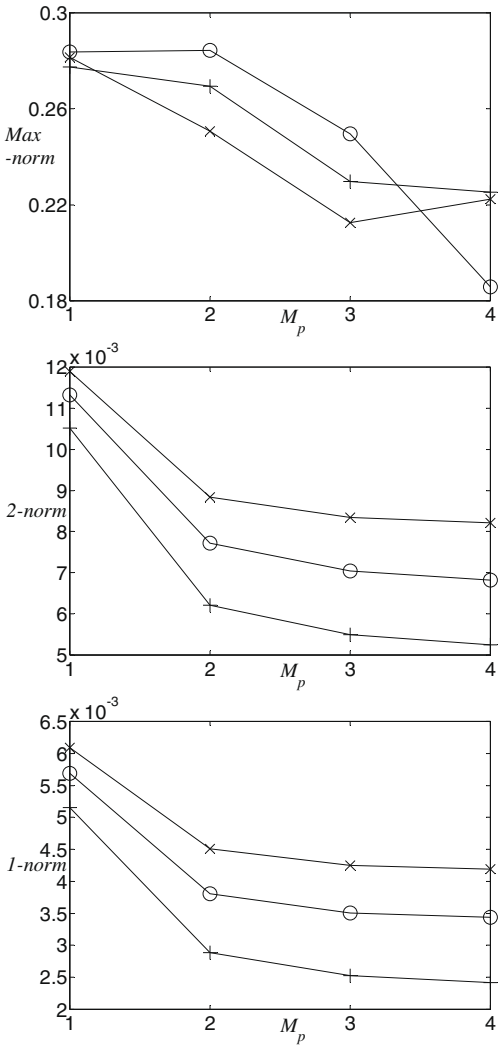

Fig. 13. Error norms of the horizontal velocity u of driven cavity flow with viscosity in random process and uncertain speed of upper plate: '×', 'o', '+' are SFDLBM results with $N_{KL} = 1, 2, 3$, respectively.

problem with μ behaving like a random process and an uncertain speed for the upper plate can be formulated. In this situation, $D = N_{KL+1}$. The problem can again be solved by specifying the same numerical and physical parameters as those given in the previous cavity flow case, and with additional specifications for $U_0 = 1$ and $U_1 = 0.25$. The results of this simulation are presented in Figs. 13–15; the error norm behavior is similar to those shown in Figs. 10–12. This example further demonstrates the viability and versatility of the SFDLBM.

6. Computational time comparison between MC and SFDLBM

Having demonstrated the viability of the SFDLBM, the next task is to assess computational economy of the SFDLBM compared to the MC simulation scheme. All SFDLBM and MC simulations are carried out in the same IBM server in the Department. In most cases attempted, the computational time for the SFDLBM is much smaller than that for the MC simulation. Table 5 reports the computer running time of the driven cavity flow and the sudden expansion flow with two random excitations. The time step (Δt) of the MC and the SFDLBM calculations are the same. For the cases of $M_p = 4$, the SFDLBM is faster than the MC method for the driven cavity flow and the sudden expansion flow cases with two random excitations, by at least 20 times and 8 times, respectively. The very significant difference in computational time between the MC calculation and the SFDLBM simulation is clearly shown. Only the computer running time of the cases with two random excitations are presented because all other cases show similar trend. It should be noted that although the system in the SFDLBM is increased by M times when compares to its deterministic counterpart (see Eq. (9)), it is observed that the computational time for the SFDLBM is not simply M times that of a single deterministic case. It is because the calculation of the summation in Eqs. (11–

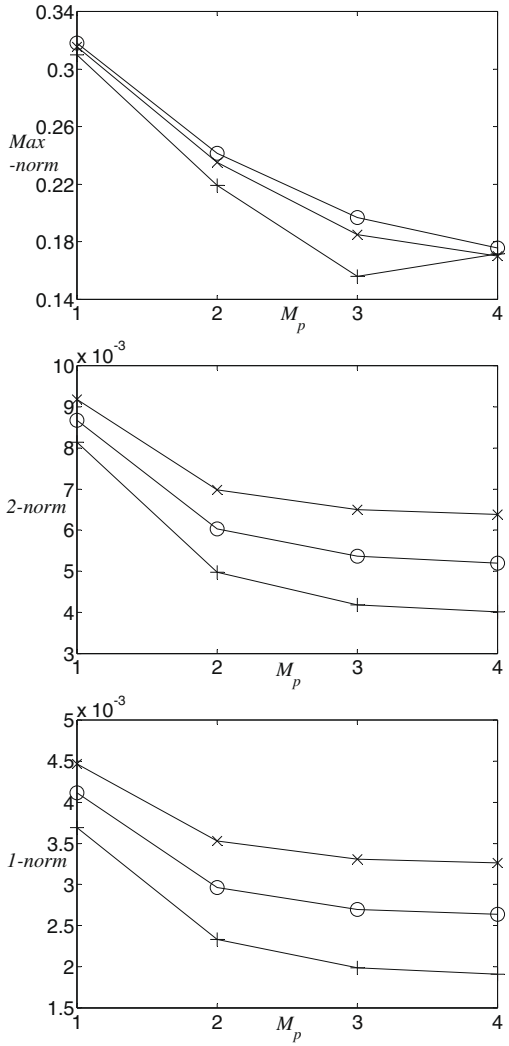

Fig. 14. Error norms of the vertical velocity v of driven cavity flow with viscosity in random process and uncertain speed of upper plate: '×', 'o', '+' are SFDLBM results with $N_{KL} = 1, 2, 3$, respectively.

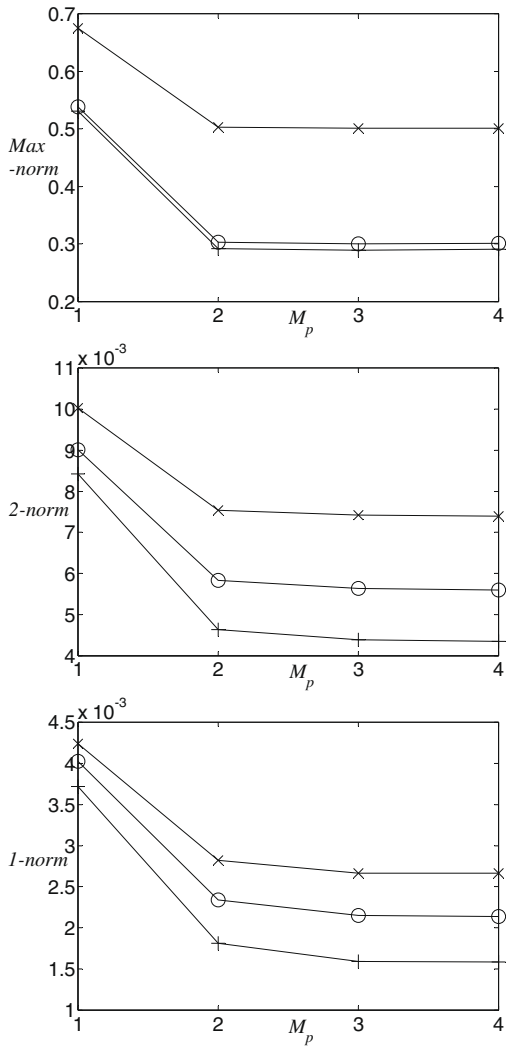

Fig. 15. Error norms of the pressure, p, of driven cavity flow with viscosity in random process and uncertain speed of upper plate: '×', 'o', '+' are SFDLBM results with N_{KL} = 1, 2, 3, respectively.

Table 5
Computer running time for the driven cavity flow and the sudden expansion flow with two random excitations.

MC scheme		Running time (h)	
		Driven cavity flow 133	Sudden expansion flow 327.5
SFDLBM scheme			
$M_p = 4$	$M = 15$	6	40.5
$M_p = 3$	$M = 10$	2.5	17
$M_p = 2$	$M = 6$	1	5.5
$M_p = 1$	$M = 3$	0.5	3

13) required additional time, and the additional time increases nonlinearly with M. This nonlinear behavior of computational time with M can be observed in Table 5.

In a random process, when $N_{KL} = M_p = 4$, and $M = 70$, it is found that the computational time for the SFDLBM becomes comparable to the calculation of the MC scheme with 1000 samples. It should be noted that the computational time for the MC scheme with 1000 samples is not just 1000 times that of calculating one sample because during a calculation, an initial condition is required for iteration until steady state is achieved. If vanishing velocity ($u = v = 0$) is used as an initial condition, the number of iteration for steady state to achieve is about two hundred thousand (∼200,000) for both deter-

ministic and stochastic simulations. In the present MC calculation, except for the first sample, which uses the vanishing velocity as an initial condition, the solution of the previous sample is used as an initial condition for the next sample calculation and this shortens the iteration process. These are the reasons why when $M = 70$, the computational time for the SFDLBM is found to be comparable to the calculation of the MC scheme with 1000 samples. However, it is not unusual for the number of samples used for the MC scheme to be over 1000. Also, the iteration time for the SFDLBM can be shortened by improving the initial guess. In most applications to solve stochastic problems, the SFDLBM still provides a much faster solution than the MC scheme. Further savings in computing time can be achieved by adapting the SFDLBM to parallel computing [4,5].

7. Conclusions

A stochastic numerical solver for steady incompressible NS equations has been developed by integrating the FDLBM with either the SSFEM or the SPM. Thus formulated, the algorithm is designated as SFDLBM. The numerical procedure of the FDLBM given in [9] and the dependent variables are projected to the Homogeneous Chaos (HC) by the expansion of the Polynomial Chaos (PC). Therefore, all advantages of the FDLBM are retained. Validation against MC solutions of channel/Couette flow, driven cavity flow, and sudden expansion flow are carried out. In these test cases, if only one source of random excitation is analyzed, the viscosity is taken to be that source. If two sources are considered, the viscosity and the velocity (or mean flow rate) are assumed to have a random component. In addition, a flow where the fluid viscosity μ is a random process is also simulated. Only a small number of terms in the PC expansion are required to ensure an accurate representation of the calculated flow field in all test cases examined. The computational resource required for the SFDLBM is found to be much reduced compared to the MC scheme.

The objective of developing the SFDLBM is to use it to simulate blood flow in micro and stenosed arteries. The complex geometry of a stenosed artery can be handled by implementing the immersed boundary (IB) method of Peskin [26] into the SFDLBM. Once successful, a SFDLBM numerical technique that can handle blood flow simulation in stenosed arteries is avail-

Table A.1
One-dimensional ($D = 1$) polynomial chaos and their variances [14].

j	Order of the homogeneous chaos, M_p	jth polynomial chaos, Ψ_j	Variance, $\langle \Psi_j^2 \rangle$
0	$M_p = 0$	$\Psi_j = 1$	$\langle \Psi_j^2 \rangle = 1$
1	$M_p = 1$	$\Psi_j = \xi_1$	$\langle \Psi_j^2 \rangle = 1$
2	$M_p = 2$	$\Psi_j = \xi_1^2 - 1$	$\langle \Psi_j^2 \rangle = 2$
3	$M_p = 3$	$\Psi_j = \xi_1^3 - 3\xi_1$	$\langle \Psi_j^2 \rangle = 6$
4	$M_p = 4$	$\Psi_j = \xi_1^4 - 6\xi_1^2 + 3$	$\langle \Psi_j^2 \rangle = 24$
5	$M_p = 5$	$\Psi_j = \xi_1^5 - 10\xi_1^3 + 15\xi_1$	$\langle \Psi_j^2 \rangle = 120$
6	$M_p = \boldsymbol{6}$	$\Psi_j = \xi_1^6 - 1\xi_1^4 + 45\xi_1^2 - 15$	$\langle \Psi_j^2 \rangle = 720$

Table A.2
Two-dimensional ($D = 2$) polynomial chaos and their variances [14].

j	Order of the homogeneous chaos, M_p	jth Polynomial chaos, Ψ_j	Variance, $\langle \Psi_j^2 \rangle$
0	$M_p = 0$	$\Psi_j = 1$	$\langle \Psi_j^2 \rangle = 1$
1	$M_p = 1$	$\Psi_j = \xi_1$	$\langle \Psi_j^2 \rangle = 1$
2		$\Psi_j = \xi_2$	$\langle \Psi_j^2 \rangle = 1$
3	$M_p = 2$	$\Psi_j = \xi_1^2 - 1$	$\langle \Psi_j^2 \rangle = 2$
4		$\Psi_j = \xi_1\xi_2$	$\langle \Psi_j^2 \rangle = 1$
5		$\Psi_j = \xi_2^2 - 1$	$\langle \Psi_j^2 \rangle = 2$
6	$M_p = 3$	$\Psi_j = \xi_1^3 - 3\xi_1$	$\langle \Psi_j^2 \rangle = 6$
7		$\Psi_j = \xi_1^2\xi_2 - \xi_2$	$\langle \Psi_j^2 \rangle = 2$
8		$\Psi_j = \xi_2^2\xi_1 - \xi_1$	$\langle \Psi_j^2 \rangle = 2$
9		$\Psi_j = \xi_2^3 - 3\xi_2$	$\langle \Psi_j^2 \rangle = 6$
10	$M_p = 4$	$\Psi_j = \xi_1^4 - 6\xi_1^2 + 3$	$\langle \Psi_j^2 \rangle = 24$
11		$\Psi_j = \xi_1^3\xi_2 - 3\xi_1\xi_2$	$\langle \Psi_j^2 \rangle = 6$
12		$\Psi_j = \xi_1^2\xi_2^2 - \xi_1^2 - \xi_2^2 + 1$	$\langle \Psi_j^2 \rangle = 4$
13		$\Psi_j = \xi_2^3\xi_1 - 3\xi_2\xi_1$	$\langle \Psi_j^2 \rangle = 6$
14		$\Psi_j = \xi_2^4 - 6\xi_2^2 + 3$	$\langle \Psi_j^2 \rangle = 24$

able. The present work demonstrates that a viable SFDLBM capable of handling a random process has been developed; therefore, it represents the first step towards the construction of a SFDLBM with IB capability.

Acknowledgments

S.C.F. gratefully acknowledges funding support in the form of a Ph.D. studentship awarded him by the Hong Kong Polytechnic University. R.M.C.S. would like to acknowledge support given to him as Co-I and Co-PI, respectively, by FAA and NSF in the form of research grants.

Appendix A. 1-D and 2-D polynomial chaoses

See Tables A.1 and A.2.

References

[1] P.L. Bhatnagar, E.P. Gross, M. Krook, A model for collision processes in gases: I. Small amplitude processes in charged and neutral one-component systems, Physical Review 94 (1954) 511–525.
[2] S. Chapman, T.G. Cowling, The Mathematical Theory of Non-uniform Gases, third ed., Cambridge University Press, 1990.
[3] S. Chen, G.D. Doolen, Lattice Boltzmann method for fluid flows, Annual Review of Fluid Mechanics 30 (1998) 329–364.
[4] G. Wellein, P. Lammers, G. Hager, S. Donath, T. Zeiser, Towards optimal performance for lattice Boltzmann applications on terascale computers, in: A. Deane et al. (Ed.), Parallel Computational Fluid Dynamics: Theory and Applications, Proceedings of the 2005 International Conference on Parallel Computational Fluid Dynamics, May 24–27, College Park, MD, USA, 2005, pp. 31–40.
[5] G. Wellein, T. Zeiser, G. Hager, S. Donath, On the single processor performance for simple lattice Boltzmann kernels, Computers and Fluids 35 (2006) 910–919.
[6] D.A. Wolf-Gladrow, Lattice-Gas Cellular Automata and Lattice Boltzmann Models. An Introduction, Springer Verlag, 2000 (Chapter 5).
[7] N.S. Cao, S. Chen, S. Jin, D. Martinez, Physical symmetry and lattice symmetry in the lattice Boltzmann method, Physical Review E 55 (1997) R21–24.
[8] R. Mei, W. Shyy, On the finite difference-based lattice Boltzmann method in curvilinear coordinates, Journal of Computational Physics 143 (1998) 426–448.
[9] S.C. Fu, W.W.F. Leung, R.M.C. So, A lattice Boltzmann method based numerical scheme for micro-channel flows, Journal of Fluids Engineering 131 (081401) (2009) 11.
[10] J.M. Hammersley, D.C. Handscomb, Monte Carlo Methods, Methuen, London, 1964.
[11] S. Wiener, The homogeneous chaos, American Journal of Mathematics 60 (1938) 897–936.
[12] R. Cameron, W. Martin, The orthogonal development of nonlinear functionals in series of Fourier–Hermite functional, Annals of Mathematics 48 (1947) 385–392.
[13] A. Chorin, Hermite expansions in Monte-Carlo computation, Journal of Computational Physics 8 (1971) 472–482.
[14] R.G. Ghanem, P.D. Spanos, Stochastic Finite Elements: A Spectral Approach, Springer-Verlag, Berlin/New York, 1991.
[15] R. Ghanem, Probabilistic characterization of transport in heterogeneous media, Computational Methods in Applied Mechanical Engineering 158 (1998) 199–220.
[16] O.P. Le Maître, O.M. Knio, H.N. Najm, R.G. Ghanem, A stochastic projection method for fluid flow I. Basic formulation, Journal of Computational Physics 173 (2001) 481–511.
[17] O.P. Le Maître, M.T. Reagan, H.N. Najm, R.G. Ghanem, O.M. Knio, A stochastic projection method for fluid flow II. Random process, Journal of Computational Physics 181 (2002) 9–44.
[18] O.P. Le Maître, O.M. Knio, H.N. Najm, R.G. Ghanem, Uncertainty propagation using Wiener–Haar expansions, Journal of Computational Physics 197 (2004) 28–57.
[19] A. Nouy, O.P. Le Maître, Generalized spectral decomposition for stochastic nonlinear problems, Journal of Computational Physics 228 (2009) 202–235.
[20] A.A. Stadler, E.P. Zilow, O. Linderkamp, Blood viscosity and optimal hematocrit in narrow tubes, Biorheology 27 (1990) 779–788.
[21] S. Chien, S. Usami, R.J. Dellenback, M.I. Gregersen, Shear dependent deformation of erythrocytes in rheology of human blood, American Journal of Physiology 219 (1970) 136–142.
[22] A.R. Pries, D. Neuhaus, P. Gaehtgens, Blood viscosity in tube flow: dependence on diameter and hematocrit, American Journal of Heart Circulatory Physiology 263 (1992) 1770–1778.
[23] G.D.O. Lowe, Blood rheology in arterial disease, Clinical Science 71 (1986) 137–146.
[24] D.N. Ku, Blood flow in arteries, Annual Review of Fluid Mechanics 29 (1997) 399–434.
[25] H. Huang, V.J. Modi, B.R. Seymour, Fluid mechanics of stenosed arteries, International Journal of Engineering Science 33 (1995) 815–828.
[26] C.S. Peskin, Numerical analysis of blood flow in the heart, Journal of Computational Physics 25 (3) (1977) 220–252.
[27] U. Ghia, K.N. Ghia, C.T. Shin, High-Re solutions for incompressible flow using the Navier–Stokes equations and a multigrid method, Journal of Computational Physics 48 (1982) 387–411.
[28] P.D. Lax, B. Wendroff, Systems of conservation laws, Communication in Pure and Applied Mathematics 13 (1960) 217–237.
[29] A. Kumar, K.S. Yajnik, Separated flows at large Reynolds numbers, Journal of Fluid Mechanics 97 (1980) 27–51.